Inorg. Chem. **2007**, *46*, 10229–10240

Inorganic Chemistry
Article

Influence of Steric Hindrance on the Core Geometry and Sulfoxidation Chemistry of Carboxylate-Rich Diiron(II) Complexes

Erwin Reisner, Tanya C. Abikoff, and Stephen J. Lippard*

Department of Chemistry, Massachusetts Institute of Technology,
Cambridge, Massachusetts 02139

Received July 16, 2007

The asymmetric terphenyl-2′-carboxylate ligand 3,5-dimethyl-1,1′:3′,1′′-terphenyl-2′-carboxylate, $^{-}O_2CAr^{Ph,Xyl}$, was prepared in high yield. This ligand facilitates the assembly of the diiron(II) complexes $[Fe_2(\mu\text{-}O_2CAr^{Tol})_2(O_2CAr^{Ph,Xyl})_2(THF)_2]$ [**2**, $^{-}O_2CAr^{Tol}$ = 2,6-di-*p*-tolylbenzoate], $[Fe_2(\mu\text{-}O_2CAr^{Tol})_2(O_2CAr^{Ph,Xyl})_2(pyridine)_2]$ (**5**), $[Fe_2(\mu\text{-}O_2CAr^{Ph,Xyl})_2(O_2CAr^{Ph,Xyl})_2(THF)_2]$ (**3**), and $[Fe_2(\mu\text{-}O_2CAr^{Ph,Xyl})_2(O_2CAr^{Ph,Xyl})_2(pyridine)_2]$ (**6**), all of which have a windmill geometry. The iron–iron distance of 3.355[10] Å in **6** is ~1 Å shorter than that in the analogue $[Fe_2(\mu\text{-}O_2CAr^{Tol})_2(O_2CAr^{Tol})_2(pyridine)_2]$ (**4**) and similar to the ~3.3 Å metal–metal separation at the active site of the reduced diiron(II) form of the soluble methane monooxygenase hydroxylase enzyme ($MMOH_{red}$). A series of ortho-substituted picolyl-based ligands, 2-picSMe, 2-picSEt, 2-picS^{t}Bu, 2-picSPh, 2-picSPh(Me_3) (Ph(Me_3) = mesityl), and 2-picSPh(^{i}Pr_3) (Ph(^{i}Pr_3) = 2,4,6-triisopropylphenyl), were prepared and allowed to react with $[Fe_2(\mu\text{-}O_2CAr)_2(O_2CAr)_2(THF)_2]$ to produce $[Fe_2(\mu\text{-}O_2CAr)_3(O_2CAr)(picSR)]$ (**7**–**13**, Ar = Ar^{Tol} or $Ar^{Ph,Xyl}$) complexes in 45–87% yields. The substrates tethered to the pyridine N-donor ligands picSR, where R = Me, Et, ^{t}Bu, or Ph, coordinate to one iron atom of the diiron(II) center by the nitrogen and sulfur atoms to form a five-membered chelate ring. The Fe–S distance becomes elongated with increasing steric hindrance imparted by the R group. The most sterically hindered ligands, 2-picSPh(Me_3) and 2-picSPh(^{i}Pr_3), bind to the metal only through the pyridine nitrogen atom. The reactions of several of these complexes with dioxygen were investigated, and the oxygenated products were analyzed by ^{1}H NMR spectroscopy and GC/MS measurements following decomposition on a Chelex resin. The amount of sulfoxidation product is correlated with the Fe···S distance. The ratio of oxidized to unoxidized thioether substrate varies from 3.5, obtained upon oxygenation of the weakly coordinated 2-picSPh ligand in **10**, to 1.0, obtained for the bulky 2-picSPh(^{i}Pr_3) ligand in **12**, for which the iron–sulfur distance is >4 Å. External thioether substrates were not oxidized when present in oxygenated solutions of paddlewheel and windmill diiron(II) complexes containing 1-methylimidazole or pyridine ligands, respectively.

Introduction

Methanotrophic bacteria live at the aerobic/anaerobic interface in the environment, where they consume methane as their sole source of carbon and energy. This process is accomplished by a multicomponent protein complex that catalyzes the selective oxidation of methane to methanol under ambient conditions.[1] Methanol holds considerable promise as a useful chemical feedstock and fuel, but its industrial production from abundant natural gas reserves via the intermediate production of synthesis gas is expensive.[2] It therefore remains of interest to discover chemistry for converting methane directly to methanol in an economical and efficient manner. Because significant progress has been made in understanding how nature catalyzes this transformation in the soluble methane monooxygenase (sMMO) from bacteria, we aim to apply the principles of dioxygen activation and hydrocarbon oxidation learned in studies of the enzyme to devise synthetic analogues capable of achieving similar chemistry.

---

* To whom correspondence should be addressed. E-mail: lippard@mit.edu.

(1) (a) Merkx, M.; Kopp, D. A.; Sazinsky, M. H.; Blazyk, J. L.; Müller, J.; Lippard, S. J. *Angew. Chem., Int. Ed.* **2001**, *40*, 2782−2807. (b) Solomon, E. I.; Brunold, T. C.; Davis, M. I.; Kemsley, J. N.; Lee, S.-K.; Lehnert, N.; Neese, F.; Skulan, A. J.; Yang, Y.-S.; Zhou, J. *Chem. Rev.* **2000**, *100*, 235−349. (c) Kovaleva, E. G.; Neibergall, M. B.; Chakrabarty, S.; Lipscomb, J. D. *Acc. Chem. Res.* **2007**, *40*, 475−483. (d) Baik, M.-H.; Newcomb, M.; Friesner, R. A.; Lippard, S. J. *Chem. Rev.* **2003**, *103*, 2385−2419.

(2) Lange, J.-P. *Ind. Eng. Chem. Res.* **1997**, *36*, 4282−4290.

10.1021/ic7014176 CCC: $37.00

Chart 1

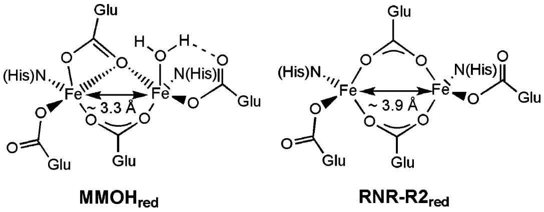

Chart 2

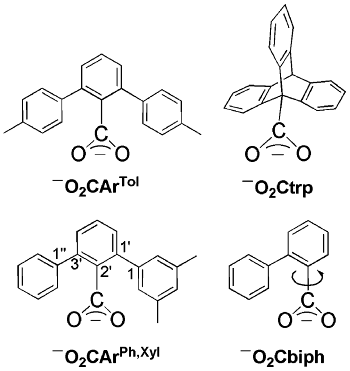

The active site of the hydroxylase component (MMOH) of sMMO features a non-heme diiron center coordinated by four glutamate and two histidine residues. The reduced diiron(II) form ($MMOH_{red}$; Chart 1) reacts directly with dioxygen, activating it for hydrocarbon oxidation. In recent years, there has been significant progress in the preparation of structural mimics of the MMOH active site.[3] In particular, the introduction of sterically hindered terphenyl-based carboxylates, such as 2,6-di-*p*-tolylbenzoate ($^-O_2CAr^{Tol}$; Chart 2) or 2,6-dimesitylbenzoate, has enabled the preparation of model compounds having a diiron(II) center and a carboxylate-rich ligand environment similar to that in MMOH.[3−6] The structures of these diiron compounds can be influenced by the steric requirements of the carboxylate and N-donor ligands, and the resulting complexes adopt a variety of forms. Included are windmill (doubly bridged), triply bridged, or paddlewheel (quadruply carboxylate-bridged) structures.[4,7] In addition to terphenylcarboxylates, triptycene ($^-O_2Ctrp$)[8] and biphenylcarboxylate ($^-O_2Cbiph$; Chart 2)[9] ligands have recently promoted the assembly of paddlewheel $[Fe_2(\mu\text{-}O_2CR)_4(\text{N-donor})_2]$ cores.

Regio- and stereoselective functionalization of nonactivated substrates by dioxygen is a primary goal in the development of methods for oxidation.[10] Biomimetic catalysts that selectively hydroxylate hydrocarbons are highly desired. In addition to selective oxidation of alkanes and arenes to alcohols, bacterial multicomponent monooxygenases also oxidize substrates such as methanethiol and organic sulfides.[11,12] Paddlewheel diiron(II) complexes with 2,6-dibenzylbenzoate type ligands react with dioxygen to afford thermally labile peroxo intermediates,[13] which are capable of oxidizing triphenylphosphine substrates.[14] A toluene monooxygenase model complex, $[Fe_2(L^{Ph4})(Ph_3CCO_2)]^{2+}$, where L^{Ph4} is *N*,*N*,*N'*,*N'*-tetrakis[(1-methyl-2-phenyl-4-imidazolyl)methyl]-1,3-diamino-2-propanolate), forms a peroxodiiron(III) intermediate upon oxygenation and hydroxylates the arene group of the supporting L^{Ph4} ligand.[15]

Previously, we reported C−H bond activation at carboxylate-bridged diiron complexes containing benzyl and/or ethyl moieties tethered to amine or pyridine ligands, as well as with thioether and sulfoxide substituents on the pyridine ligands in the ortho position.[16−19] Oxidation to alcohols, aldehydes, sulfoxides, and sulfones occurred for substrates tethered in close proximity to the diiron(II) center. No oxidation occurred with substrate moieties tethered to the meta or para position of a pyridine ligand, demonstrating the importance of proximity to the diiron center. In one instance, a mechanistic study indicated that oxidative N-dealkylation in $[Fe_2(\mu\text{-}O_2CAr^{Tol})_2(O_2CAr^{Tol})_2$(*N*,*N*-dibenzylethylenediamine$)_2]$ involves one-electron transfer from a nitrogen atom to a transient electrophilic diiron intermediate followed by proton transfer and rearrangement to eliminate benzaldehyde.[20]

Here we describe a novel asymmetric terphenylcarboxylate ligand ($^-O_2CAr^{Ph,Xyl}$; Chart 2) and a series of diiron complexes containing this unit as well as N-donor ligands with tethered thioether substrates. The ability of $^-O_2CAr^{Ph,Xyl}$ to influence the structural properties of these synthetic MMOH models is delineated. The asymmetric carboxylate ligand was designed in order to assemble diiron(II) complexes having shorter Fe−Fe distances and the potential to accommodate a single-atom-bridged diiron(II) motif (Chart 1). The oxidation of the tethered substrates following the addition of dioxygen to diiron(II) complexes containing $^-O_2CAr^{Ph,Xyl}$ and $^-O_2CAr^{Tol}$ (Chart 2) was investigated. 2-Picolyl-based thioether substrates were chosen to compare methylenic C−H bond activation vs sulfoxidation for a variety of substrates having either coordinated or freely “dangling” thioether moieties.

---

(3) Tshuva, E. Y.; Lippard, S. J. *Chem. Rev.* **2004**, *104*, 987−1012.
(4) Tolman, W. B.; Que, L., Jr. *J. Chem. Soc., Dalton Trans.* **2002**, 653−660.
(5) Hagadorn, J. R.; Que, L., Jr.; Tolman, W. B. *J. Am. Chem. Soc.* **1998**, *120*, 13531−13532.
(6) Lee, D.; Lippard, S. J. *J. Am. Chem. Soc.* **1998**, *120*, 12153−12154.
(7) Lee, D.; Lippard, S. J. *Inorg. Chem.* **2002**, *41*, 2704−2719.
(8) Friedle, S.; Kodanko, J. J.; Fornance, K. L.; Lippard, S. J. Manuscript in preparation, 2007.
(9) Reisner, E.; Telser, J.; Lippard, S. J. *Inorg. Chem.* **2007**, In press.
(10) Du Bois, J.; Mizoguchi, T. J.; Lippard, S. J. *Coord. Chem. Rev.* **2000**, *200−202*, 443−485.
(11) Fuse, H.; Ohta, M.; Takimura, O.; Murakami, K.; Inoue, H.; Yamaoka, Y.; Oclarit, J. M.; Omori, T. *Biosci., Biotechnol., Biochem.* **1998**, *62*, 1925−1931.
(12) Colby, J.; Stirling, D. I.; Dalton, H. *Biochem. J.* **1977**, *165*, 395−402.
(13) Chavez, F. A.; Ho, R. Y. N.; Pink, M.; Young, V. G., Jr.; Kryatov, S. V.; Rybak-Akimova, E. V.; Andres, H.; Münck, E.; Que, L., Jr.; Tolman, W. B. *Angew. Chem., Int. Ed.* **2002**, *41*, 149−152.
(14) Kryatov, S. V.; Chavez, F. A.; Reynolds, A. M.; Rybak-Akimova, E. V.; Que, L.; Jr.; Tolman, W. B. *Inorg. Chem.* **2004**, *43*, 2141−2150.
(15) Yamashita, M.; Furutachi, H.; Tosha, T.; Fujinami, S.; Saito, W.; Maeda, Y.; Takahashi, K.; Tanaka, K.; Kitagawa, T.; Suzuki, M. *J. Am. Chem. Soc.* **2007**, *129*, 2−3.
(16) Carson, E. C.; Lippard, S. J. *J. Am. Chem. Soc.* **2004**, *126*, 3412−3413.
(17) Carson, E. C.; Lippard, S. J. *Inorg. Chem.* **2006**, *45*, 837−848.
(18) Carson, E. C.; Lippard, S. J. *Inorg. Chem.* **2006**, *45*, 828−836.
(19) Carson, E. C.; Lippard, S. J. *J. Inorg. Biochem.* **2006**, *100*, 1109−1117.
(20) (a) Yoon, S.; Lippard, S. J. *Inorg. Chem.* **2003**, *42*, 8606−8608. (b) Yoon, S.; Lippard, S. J. *Inorg. Chem.* **2006**, *45*, 5438−5446.

Experimental Section

Materials and Methods. All reagents were obtained from commercial suppliers and used as received unless otherwise noted. Dichloromethane, pentane, and diethyl ether for the preparation of diiron(II) complexes were saturated with nitrogen and purified by passage through activated Al_2O_3 columns under argon gas. Anhydrous chlorobenzene was used to recrystallize the diiron(II) compounds. Thioether ligands were prepared in anhydrous dimethyl sulfoxide (DMSO) containing powdered, dry KOH. Macroporous polystyrene-2,4,6-trimercaptotriazine (MP−TMT) was obtained from Argonaut Technologies. 3-Iodobiphenyl-2-carboxylic acid[21] and 2,4,6-triisopropylbenzenethiol[22] were prepared as described previously. The reagents $Fe(OTf)_2 \cdot 2MeCN$,[23] $[Fe_2(\mu\text{-}O_2CAr^{Tol})_2(O_2CAr^{Tol})_2(THF)_2]\cdot 2CH_2Cl_2$[6] (**1**), and $[Fe_2(\mu\text{-}O_2CAr^{Tol})_2(O_2CAr^{Tol})_2(pyridine)_2]$[6] (**4**) were synthesized as reported in the literature, and their identities were confirmed by single-crystal X-ray diffraction. All diiron(II) complexes were prepared under dinitrogen in an MBraun drybox. Dioxygen (99.994%, BOC Gases) was dried by passing the gas stream through a column of Drierite.

3-Iodobiphenyl-2-carboxylic acid. The compound was obtained in 70% yield. ^1H NMR (300 MHz, CD_3OD) δ: 7.84 (dd, J = 7.8 and 0.9 Hz, 1H), 7.38−7.30 (m, 6H), 7.16 (t, J = 7.5 Hz, 1H). ^{13}C NMR (300 MHz, DMSO-d_6) δ: 172.71, 142.28, 142.12, 141.24, 139.36, 131.65, 130.81, 129.73, 129.51, 129.17, 92.75. R_f = 0.39 (hexane/EtOAc = 5/5). ESI-MS (m/z, MeOH). Calcd for $[M - H]^-$: 323.0. Found: 323.0. Calcd for $[M + Na]^+$ 347.0. Found: 347.1. IR (KBr, cm^{-1}) ν(C=O): 1707 (s), 1692 (s). Mp: 172−173 °C.

Methyl 3-Iodobiphenyl-2-carboxylate. Cs_2CO_3 (8.76 g, 26.9 mmol) and methyl iodide (2.08 mL, 33.60 mmol) were added to a solution of 3-iodobiphenyl-2-carboxylic acid (7.26 g, 22.4 mmol) in *N*,*N*-dimethylformamide (DMF; 30 mL). The suspension was stirred for 0.5 h at room temperature, after which CH_2Cl_2 (200 mL) was added. The mixture was washed with aqueous $NaHCO_3$ (2 × 100 mL) and H_2O (150 mL). The organic phase was dried with $MgSO_4$, filtered, and concentrated to dryness. Removal of the solvent under vacuum at 60 °C resulted in the formation of a white powder. Yield: 7.20 g, 95%. ^1H NMR (300 MHz, CD_3OD) δ: 7.84 (dd, J = 7.8 and 1.2 Hz, 1H), 7.40−7.26 (m, 6H), 7.19 (t, J = 7.8 Hz, 1H), 3.59 (s, 3H). ^{13}C NMR (300 MHz, DMSO-d_6) δ: 168.83, 140.54, 139.01, 138.78, 137.78, 131.39, 129.43, 128.63, 128.13, 127.95, 93.59, 52.36. R_f = 0.63 (hexane/EtOAc = 8/2). ESI-MS (m/z, MeOH). Calcd for $[M + Na]^+$ 361.0. Found: 360.9. Calcd for $[2M + Na]^+$ 698.9. Found: 698.7. IR (KBr, cm^{-1}) ν(C=O): 1734 (s). Mp: 89−90 °C.

Methyl 3,5-Dimethyl-1,1′:3′,1′′-terphenyl-2′-carboxylate. 3,5-Dimethylphenylboronic acid (3.30 g, 1.5 equiv) was added to methyl 3-iodobiphenyl-2-carboxylate (5.00 g, 14.8 mmol) dissolved in tetrahydrofuran (THF; 100 mL) and 1 M aqueous Na_2CO_3 (40 mL). The reaction mixture was deoxygenated by bubbling with argon for 20 min, after which $[PdCl_2(PPh_3)_2]$ (5 mol %, 0.52 g, 0.74 mmol) was added. The reaction mixture was purged with argon for an additional 10 min and heated to 60 °C. The orange reaction mixture turned yellow after ca. 0.5 h and black overnight. The resulting dark reaction mixture was cooled to room temperature and added to water (200 mL), and the product was extracted with CH_2Cl_2 (2 × 200 mL). The combined organic phases were dried with $MgSO_4$ and concentrated to dryness. The product was purified by column chromatography (SiO_2, CH_2Cl_2/hexane = 3/7) to give a white powder. Trace palladium (indicated by a yellow tint) was removed by stirring the product overnight in dichloromethane with MP−TMT (a Pd scavenger) at room temperature. Yield: 3.85 g, 81%. ^1H NMR (300 MHz, DMSO-d_6) δ: 7.60 (dd, 1H), 7.48−7.31 (m, 7H), 7.02 (s, 1H), 6.95 (s, 2H), 3.33 (s, 3H), 2.30 (s, 6H). ^{13}C NMR (300 MHz, DMSO-d_6) δ: 169.3, 140.0, 139.9, 139.7, 139.5, 137.5, 132.2, 129.8, 129.1, 128.8, 128.7, 128.5, 128.1, 127.7, 125.9, 51.6, 21.0. R_f = 0.56 (CH_2Cl_2/hexane = 5/5). ESI-MS (m/z, MeOH). Calcd for $[M + Na]^+$: 339.1. Found: 339.1. Calcd for $[2M + Na]^+$ 655.3. Found: 655.1. IR (KBr, cm^{-1}) ν(C=O): 1730 (vs). Mp: 119−120 °C.

3,5-Dimethyl-1,1′:3′,1′′-terphenyl-2′-carboxylic Acid. Methyl 3,5-dimethyl-1,1′:3′,1′′-terphenyl-2′-carboxylate (2.00 g, 6.33 mmol) and lithium iodide (6.36 g, 47.44 mmol) were dissolved in anhydrous pyridine (80 mL). The reaction mixture was heated in a pressure vessel under a dinitrogen atmosphere at 120 °C for 6 days and protected from light with aluminum foil. A yellowish solution formed that was poured into 6 M HCl (600 mL) cooled at 0 °C, and the product was extracted from the aqueous phase with $CHCl_3$ (2 × 300 mL). The combined organic phases were washed with water (2 × 300 mL), dried with Na_2SO_4, and concentrated to dryness. The white powder was dried under high vacuum at 60 °C. Yield: 1.75 g, 92%. ^1H NMR (300 MHz, DMSO-d_6) δ: 12.79 (s, 1H), 7.53 (t, J = 7.5 Hz, 1H), 7.46−7.31 (m, 7H), 7.03 (s, 2H), 7.02 (s, 1H), 2.29 (s, 6H). ^{13}C NMR (300 MHz, $CDCl_3$) δ: 174.5, 140.8, 140.6(2), 140.3, 138.1, 131.5, 129.8, 129.5, 129.2, 129.0, 128.5(2), 127.8, 126.4, 21.5. ESI-MS (m/z, MeOH). Calcd for $[M + Na]^+$: 325.1. Found: 325.0. Calcd for $[M - H]^-$: 301.1. Found: 300.9. IR (KBr, cm^{-1}) ν(C=O): 1690 (s). Mp: 194−195 °C.

Sodium 3,5-Dimethyl-1,1′:3′,1′′-terphenyl-2′-carboxylate. A solution of 3,5-dimethyl-1,1′:3′,1′′-terphenyl-2′-carboxylic acid (1.75 g, 5.79 mmol) and NaOH (232 mg, 5.79 mmol) in MeOH (100 mL) was heated at 60 °C for 3 h. The resulting mixture was concentrated to dryness to afford a white powder that was dried at 60 °C under high vacuum overnight. Yield: 1.88 g, quant. ^1H NMR (300 MHz, CD_3OD) δ: 7.51 (d, J = 8.4 Hz, 2H), 7.30−7.10 (m, 8H), 6.85 (s, 1H), 2.24 (s, 6H). ^{13}C NMR (300 MHz, DMSO-d_6) δ: 172.1, 142.6, 142.5, 136.8, 136.3, 136.2, 128.7, 128.3, 128.1, 127.8, 127.7, 127.6, 126.6, 126.2, 124.8, 21.1. ESI-MS (m/z, MeOH). Calcd for $[M - Na]^-$: 301.1. Found: 301.2. Calcd for $[2M - Na]^-$: 625.2. Found: 625.4. Calcd for $[M + Na]^+$: 347.1. Found: 347.2. Calcd for $[2M + Na]^+$: 671.2. Found: 671.2. IR (KBr, cm^{-1}) ν(C=O): 1601 (m), 1578 (s). Mp: >300 °C.

Synthesis of Picolyl Thioethers and Sulfoxides: General Procedure. The picolyl-based thioethers were prepared in a manner similar to that described in the literature.[24,25] 2-Picolylchloride hydrochloride (1.0 g, 6.1 mmol) was added to a stirred suspension of KOH (3.0 g, 53.5 mmol) in DMSO (15 mL) containing 1.1 equiv (6.7 mmol) of 2-methylpropane-2-thiol, benzenethiol, 2,4,6-trimethylbenzenethiol, 2,4,6-triisopropylbenzenethiol, sodium methanethiolate, or sodium ethanethiolate. The suspension was stirred for 1−2 h, and H_2O (25 mL) was added. The mixture was extracted with diethyl ether (2 × 25 mL), and the combined organic phases were washed with H_2O (25 mL) and concentrated to dryness. The thioether ligands were purified by flash chromatography (SiO_2) with a mixture of ethyl acetate and hexane. 2-[(Methylsulfanyl)methyl]-

---

[21] Tilly, D.; Samanta, S. S.; Faigl, F.; Mortier, J. *Tetrahedron Lett.* **2002**, *43*, 8347−8350.

[22] Blower, P. J.; Dilworth, J. R.; Hutchinson, J.; Nicholson, T.; Zubieta, J. A. *J. Chem. Soc., Dalton Trans.* **1985**, 2639−2645.

[23] Hagen, K. S. *Inorg. Chem.* **2000**, *39*, 5867−5869.

[24] Canovese, L.; Visentin, F.; Uguagliati, P.; Chessa, G.; Pesce, A. *J. Organomet. Chem.* **1998**, *566*, 61−71.

[25] Johnstone, R. A. W.; Rose, M. E. *Tetrahedron* **1979**, *35*, 2169−2173.

pyridine[26] (yield: 75%), 2-[(ethylsulfanyl)methyl]pyridine[27] (yield: 72%), 2-[(*tert*-butylsulfanyl)methyl]pyridine[24] (yield: 76%), and 2-[(phenylsulfanyl)methyl]pyridine[27] (yield: 88%) were prepared as described above and were characterized as described previously. The picolyl-based ether ligand 2-(ethoxymethyl)pyridine (picOEt) was prepared in a manner similar to that described for the thioethers (see above), but in situ generated sodium ethanolate was used instead of sodium thiolate. The picolyl-based sulfoxides were prepared as described in the literature for similar compounds.[28]

2-[(Ethoxy)methyl]pyridine, picOEt. This compound was purified by flash chromatography (SiO_2) with ethyl acetate to yield a yellow oil. Yield: 58%. ^{1}H NMR (300 MHz, $CDCl_3$) δ: 8.56 ($H^{6,pyr}$, d, $J = 2.7$ Hz, 1H), 7.71 ($H^{4,pyr}$, t, $J = 4.7$ Hz, 1H), 7.46 (H^{pyr}, d, $J = 4.5$ Hz ,1H), 7.20 (H^{pyr}, d, $J = 3.6$ Hz, 1H), 4.65 (pyCH_2O, s, 2H), 2.65 (OCH_2Me, q, $J = 4.2$ Hz, 2H), 1.30 (CH_3, t, $J = 4.2$ Hz, 3H). $R_f = 0.45$ (hexane/ethyl acetate = 2/8). ESI-MS (*m*/*z*, MeOH). Calcd for $[M + H]^+$: 138.1. Found: 138.8. Calcd for $[M + Na]^+$: 160.1. Found: 160.5. IR (KBr, cm^{-1}) selected bands: 2978 (m), 1734 (s), 1719 (s), 1586 (m), 1369 (m), 1308 (s), 1246 (m), 1131 (s), 750 (s), 708 (s).

2-[(Mesitylsulfanyl)methyl]pyridine, picSPh(Me_3). This compound was purified by flash chromatography (SiO_2) with hexane/ethyl acetate (7/3) as a colorless oil. Yield: 88%. ^{1}H NMR (300 MHz, $CDCl_3$) δ: 8.52 ($H^{6,pyr}$, d, $J = 4.8$ Hz, 1H), 7.52 ($H^{4,pyr}$, t, $J = 7.8$ Hz, 1H), 7.13 (H^{pyr}, dd, $J = 7.5$ and 4.8 Hz, 1H), 6.90 (H^{pyr}, d, $J = 7.8$ Hz, 1H), 6.89 (H^{benz}, s, 2H), 3.91 (CH_2S, s, 2H), 2.33 ($H^{Me,ortho}$, s, 6H), 2.26 ($H^{Me,para}$, s, 3H). $R_f = 0.47$ (hexane/ethyl acetate = 7/3). ESI-MS (*m*/*z*, MeOH). Calcd for $[M + H]^+$: 244.4. Found: 245.0. IR (KBr, cm^{-1}) selected bands: 2970 (m), 2927 (m), 1590 (s), 1436 (s), 993 (m), 851 (s), 752 (s), 683 (m).

2-[(2,4,6-Triisopropylphenylsulfanyl)methyl]pyridine, picSPh(^{i}Pr$_3$). This compound was purified by flash chromatography (SiO_2) with hexane/ethyl acetate (8/2) and isolated as a white powder. Yield: 86%. ^{1}H NMR (300 MHz, $CDCl_3$) δ: 8.57 ($H^{6,pyr}$, d, $J = 4.2$ Hz, 1H), 7.52 ($H^{4,pyr}$, dt, $J = 1.5$ and 7.8 Hz, 1H), 7.14 (H^{pyr}, dd, $J = 4.8$ and 7.5 Hz, 1H), 6.99 (H^{benz}, s, 2H), 6.93 (H^{pyr}, d, $J = 8.1$ Hz, 1H), 3.93 (CH_2S, s, 2H), 3.80 (Me_2CH^{ortho}, septet, $J = 6.9$ Hz, 2H), 2.88 (Me_2CH^{para}, septet, $J = 6.9$ Hz, 1H), 1.26 ($H^{Me,para}$, d, $J = 6.9$ Hz, 6H), 1.16 ($H^{Me,ortho}$, d, $J = 7.2$ Hz, 12 H). $R_f = 0.52$ (hexane/ethyl acetate = 8/2). ESI-MS (*m*/*z*, MeOH). Calcd for $[M + H]^+$: 328.2. Found: 328.0. IR (KBr, cm^{-1}) selected bands: 2959 (s), 2924 (m), 2865 (m), 1595 (s), 1465 (s), 1431 (s), 1360 (m), 1059 (m), 886 (m) 763 (m), 747 (m). Mp: 84−85 °C.

2-[(Phenylsulfinyl)methyl]pyridine, picS(O)Ph. The synthesis of this compound was reported previously.[29] It was isolated as a colorless oil. Yield: 78%. ^{1}H NMR (300 MHz, CD_3OD) δ: 8.48 ($H^{6,pyr}$, d, $J = 4.8$ Hz, 1H), 7.77 ($H^{4,pyr}$, dt, $J = 1.8$ and 7.8 Hz, 1H), 7.6−7.5 (m, 5H), 7.37 (ddd, $J = 0.9$, 4.8, and 7.5 Hz, 1H), 7.25 (td, $J = 0.9$ and 8.7 Hz, 1H), 4.33 (s, 2H). $R_f = 0.30$ (ethyl acetate). ESI-MS (*m*/*z*, MeOH). Calcd for $[M + Na]^+$: 240.0. Found: 239.9. Calcd for $[2M + Na]^+$: 457.1. Found: 456.9. IR (KBr, cm^{-1}) ν(S═O): 1044 (s).

2-[(Mesitylsulfinyl)methyl]pyridine, picS(O)Ph(Me_3). This compound was purified by flash chromatography (SiO_2) with hexane/ethyl acetate (1/9) as a white powder. Yield: 63%. ^{1}H NMR (300 MHz, $CDCl_3$) δ: 8.57 ($H^{6,pyr}$, d, $J = 3.9$ Hz, 1H), 7.60 ($H^{4,pyr}$, td, $J = 7.8$ and 1.8 Hz, 1H), 7.22 (H^{pyr}, dd, $J = 5.1$ and 7.5 Hz, 1H), 7.12 (H^{pyr}, d, $J = 7.8$ Hz, 1H), 6.83 (H^{benz}, s, 2H), 4.59 [CH_2S(O), d, $J = 12.0$ Hz, 1H], 4.38 [CH_2S(O), d, $J = 12.0$ Hz, 1H], 2.43 (CH_3^{ortho}, s, 6H), 2.28 (CH_3^{para}, s, 3H). Variable-temperature (VT) ^{1}H NMR showed that the coalescence temperature for the methylene protons is higher than 150 °C. $R_f = 0.39$ (ethyl acetate). ESI-MS (*m*/*z*, MeOH). Calcd for $[M + Na]^+$: 282.1. Found: 281.9. Calcd for $[2M + Na]^+$: 541.2. Found: 541.0. IR (KBr, cm^{-1}) ν(S═O): 1062 (s), 1043 (s). Mp: 86−88 °C.

2-[(2,4,6-Triisopropylphenylsulfinyl)methyl]pyridine, picS(O)Ph(^{i}Pr$_3$). This compound was purified by flash chromatography (SiO_2) with hexane/ethyl acetate (4/6) and obtained as a white powder. Yield: 78%. ^{1}H NMR (300 MHz, $CDCl_3$) δ: 8.61 ($H^{6,pyr}$, d, $J = 4.8$ Hz, 1H), 7.59 ($H^{4,pyr}$, t, $J = 7.8$ Hz, 1H), 7.21 (H^{pyr}, dd, $J = 4.8$ and 7.5 Hz, 1H), 7.11 (H^{pyr}, d, $J = 7.8$ Hz, 1H), 7.06 (H^{benz}, s, br, 2H), 4.71 [CH_2S(O), d, $J = 12.3$ Hz, 1H], 4.37 [CH_2S(O), d, $J = 12.3$ Hz, 1H], 2.88 (Me_2CH^{para}, septet, $J = 6.9$ Hz, 1H), 1.32−1.10 (Me_2CH^{ortho}, $CH_3^{ortho,para,}$ m, 20 H). VT ^{1}H NMR showed that the coalescence temperature for the methylene protons is higher than 150 °C. $R_f = 0.53$ (hexane/ethyl acetate: 2/8). ESI-MS (*m*/*z*, MeOH). Calcd for $[M + H]^+$: 344.2. Found: 344.2. Calcd for $[2M + Na]^+$: 709.4. Found: 709.1. IR (KBr, cm^{-1}) ν(S═O): 1043 (s), 1029 (s). Mp: 83−84 °C.

Synthesis of Diiron(II) Complexes. $[Fe_2(\mu_2\text{-}O_2CAr^{Tol})_2(O_2CAr^{Ph,Xyl})_2(THF)_2]$ (2). A portion of $Fe(OTf)_2 \cdot 2MeCN$ (337 mg, 0.77 mmol) was added to NaO_2CAr^{Tol} (250 mg, 0.77 mmol) and $NaO_2CAr^{Ph,Xyl}$ (250 mg, 0.77 mmol), suspended in THF (15 mL), and stirred at room temperature overnight. The resulting pale-yellow solution was concentrated to dryness. The product was extracted into CH_2Cl_2 (10 mL), filtered from a white powder (NaOTf), and exposed to pentane vapor diffusion. After several days, the resulting colorless blocks were washed with pentane and dried under high vacuum at room temperature. Yield: 360 mg, 64%. X-ray diffraction quality single crystals were selected directly from the reaction vessel, yielding **2**·2CH_2Cl_2. Anal. Calcd for **2**·0.75CH_2Cl_2, $C_{92.75}H_{85.5}Cl_{1.5}Fe_2O_{10}$ ($M_r = 1525.03$ g/mol): C, 73.05; H, 5.65. Found: C, 72.94; H, 5.94. IR (KBr, cm^{-1}): 3053 (w), 3022 (w), 2953 (m), 2918 (m), 2860 (w), 1602 (s), 1544 (m), 1514 (w), 1457 (m), 1413 (w), 1384 (s), 1038 (m), 858 (m), 801 (m), 765 (m), 702 (m), 544 (w), 519 (w), 452 (m). Mp: 140−143 °C (dec).

$[Fe_2(\mu_2\text{-}O_2CAr^{Ph,Xyl})_2(O_2CAr^{Ph,Xyl})_2(THF)_2]$ (3). A portion of $Fe(OTf)_2 \cdot 2MeCN$ (337 mg, 0.77 mmol) was added to $NaO_2CAr^{Ph,Xyl}$ (500 mg, 1.54 mmol), suspended in THF (15 mL), and stirred at room temperature overnight. The resulting pale-yellow solution was concentrated to dryness. The product was extracted into CH_2Cl_2 (10 mL), filtered away from a white powder (NaOTf), and exposed to pentane vapor diffusion. After several days, the resulting colorless blocks were washed with pentane and dried under high vacuum at room temperature. Yield: 270 mg, 48%. X-ray diffraction quality single crystals were selected directly from the reaction vessel, yielding **3**·0.5CH_2Cl_2. Anal. Calcd for **3**·0.25CH_2Cl_2, $C_{92.25}H_{84.5}Cl_{0.5}Fe_2O_{10}$ ($M_r = 1482.57$ g/mol): C, 74.73; H, 5.74. Found: C, 74.69; H, 5.74. IR (KBr, cm^{-1}): 3053 (m), 3018 (m), 2975 (m), 2915 (m), 2861 (w), 1599 (s), 1551 (s), 1495 (m), 1460 (s), 1440 (s), 1387 (s), 1176 (w), 1146 (w), 1038 (s), 911 (w), 886 (m), 858 (s), 814 (s), 789 (m), 765 (s), 703 (s), 626 (m). Mp: 144−148 °C (dec).

$[Fe_2(\mu_2\text{-}O_2CAr^{Tol})_2(O_2CAr^{Ph,Xyl})_2(py)_2]$ (5). Pyridine (5.6 mg, 142 μmol) in CH_2Cl_2 (1 mL) was added dropwise to a stirred suspension of **2** (100 mg, 64 μmol) in CH_2Cl_2 (4 mL) at room temperature. After 20 min, the yellow solution was layered with pentane and pale-yellow crystals formed within several days. The product was washed with pentane and dried at room temperature

---

[26] Holland, H. L.; Turner, C. D.; Andreana, P. R.; Nguyen, D. *Can. J. Chem.* **1999**, *77*, 463−471.

[27] Canovese, L.; Visentin, F.; Uguagliati, P.; Chessa, G.; Lucchini, V.; Bandoli, G. *Inorg. Chim. Acta* **1998**, *275*−*276*, 385−394.

[28] Ravikumar, K. S.; Zhang, Y. M.; Bégué, J.-P.; Bonnet-Delpon, D. *Eur. J. Org. Chem.* **1998**, 2937−2940.

[29] Cattalini, L.; Chessa, G.; Marangoni, G.; Pitteri, B.; Tobe, M. L. *J. Chem. Soc., Dalton Trans.* **1985**, 2091−2094.

under high vacuum. Yield: 50 mg, 53%. X-ray diffraction quality single crystals were grown from a diluted solution of the product in CH_2Cl_2 with slow vapor diffusion of pentane, yielding **5**·4CH_2Cl_2. Anal. Calcd for **5**·0.75CH_2Cl_2, $C_{94.75}H_{79.5}Cl_{1.5}Fe_2N_2O_8$ (M_r = 1539.02 g/mol): C, 73.94; H, 5.21; N, 1.82. Found: C, 73.81; H, 5.34; N, 1.81. IR (KBr, cm^{-1}): 3049 (w), 3022 (w), 2954 (w), 2917 (m), 2860 (w), 1604 (s), 1551 (w), 1514 (w), 1446 (m), 1383 (s), 1068 (m), 1041 (w), 855 (m), 816 (w), 802 (m), 787 (w), 759 (m), 701 (s), 627 (w), 544 (m), 531 (m). Mp: 178−182 °C (dec).

$[Fe_2(\mu_2\text{-}O_2CAr^{Ph,Xyl})_2(O_2CAr^{Ph,Xyl})_2(py)_2]$ (6). Pyridine (5.6 mg, 142 μmol) in CH_2Cl_2 (1 mL) was added dropwise to a stirred suspension of **3** (100 mg, 64 μmol) in CH_2Cl_2 (4 mL) at room temperature. After 20 min, the yellow solution was stripped to dryness and the resulting solid was recrystallized from toluene (3 mL) in contact with a layer of pentane. After several days, the resulting yellow blocks were washed with pentane and dried at room temperature under high vacuum. Yield: 84 mg, 87%. X-ray diffraction quality single crystals were grown from a solution of the product in CH_2Cl_2 with slow vapor diffusion of pentane. Anal. Calcd for **6**·0.25CH_2Cl_2, $C_{94.25}H_{78.5}Cl_{0.5}Fe_2N_2O_8$ (M_r = 1496.56 g/mol): C, 75.64; H, 5.29; N, 1.87. Found: C, 75.88; H, 5.58; N, 1.56. IR (KBr, cm^{-1}): 3057 (m), 3020 (m), 2913 (m), 1602 (s), 1547 (s), 1447 (m), 1424 (w), 1383 (s), 1068 (w), 1040 (w), 854 (m), 813 (m), 189 (m), 758 (s), 701 (s), 679 (w), 626 (m), 532 (m). Mp: 188−191 °C (dec).

General Procedure for Preparing 7−14. The corresponding picolyl-based thioether (**7**−**13**) or ether (**14**) (120 μmol) was added to a stirred suspension of $[Fe_2(\mu\text{-}O_2CAr)_2(O_2CAr)_2(THF)_2]$·2$CH_2Cl_2$ (163 mg, 100 μmol, Ar = $^{-}O_2CAr^{Tol}$ or $^{-}O_2CAr^{Ph,Xyl}$) in CH_2Cl_2 (5 mL). The resulting yellow solution formed immediately and was stirred for 0.5 h at room temperature.

$[Fe_2(\mu\text{-}O_2CAr^{Tol})_3(O_2CAr^{Tol})(picSMe)]$ (7). The product was crystallized from diethyl ether vapor diffusion into a CH_2Cl_2 solution, affording yellow blocks, which were washed with pentane and dried at room temperature. Yield: 77 mg, 50%. X-ray diffraction quality single crystals were grown from vapor diffusion of diethyl ether into a saturated CH_2Cl_2 solution of the complex, yielding **7**·CH_2Cl_2·Et_2O. Anal. Calcd for **7**·CH_2Cl_2, $C_{92}H_{79}NCl_2O_8SFe_2$ (M_r = 1541.31 g/mol): C, 71.69; H, 5.17; N, 0.91. Found: C, 71.72; H, 5.35; N, 1.04. IR (KBr, cm^{-1}): 3047 (w), 3021 (w), 2948 (w), 2918 (m), 2854 (w), 1601 (s), 1514 (m), 1453 (s), 1408 (m), 1383 (s), 1020 (m), 658 (w), 817 (m), 798 (s), 765 (m), 738 (w), 713 (w), 703 (w), 584 (w), 530 (m). Mp: 139−143 °C (dec).

$[Fe_2(\mu\text{-}O_2CAr^{Tol})_3(O_2CAr^{Tol})(picSEt)]$ (8). Pentane vapor diffusion into a CH_2Cl_2 solution of the compound yielded yellow needle-shaped blocks within 1 week, which were washed with pentane and dried at room temperature. Yield: 85 mg, 56%. X-ray diffraction quality single crystals were selected directly from the reaction vessel, yielding **8**·2CH_2Cl_2. Anal. Calcd for **8**·0.5CH_2Cl_2, $C_{92.5}H_{80}NClO_8SFe_2$ (M_r = 1512.84 g/mol): C, 73.44; H, 5.33; N, 0.93; S, 2.12. Found: C, 73.33; H, 5.18; N, 0.85; S, 2.15. IR (KBr, cm^{-1}): 3054 (w), 3017 (w), 2919 (m), 2857 (w), 1602 (s), 1577 (w), 1538 (w), 1514 (m), 1453 (m), 1407 (w), 1384 (s), 1019 (w), 860 (w), 845 (w), 835 (w), 817 (m), 798 (s), 784 (w), 770 (w), 737 (w), 715 (m), 703 (m), 584 (w), 531 (m). Mp: 141−143 °C (dec).

$[Fe_2(\mu\text{-}O_2CAr^{Tol})_3(O_2CAr^{Tol})(picS^tBu)]$ (9). The solution was evaporated to dryness, and compound **9** was recrystallized from CH_2Cl_2 with pentane vapor diffusion. After 1 week, the resulting yellow blocks were washed with pentane and dried at room temperature. Yield: 69 mg, 45%. X-ray diffraction quality single crystals were grown by layering a saturated chlorobenzene/dichloromethane solution of the complex with pentane, yielding **9**·C_6H_5Cl·0.25pentane. Anal. Calcd for **9**·0.5CH_2Cl_2, $C_{94.5}H_{84}NClO_8SFe_2$ (M_r = 1540.89 g/mol): C, 73.66; H, 5.49; N, 0.91; S, 2.08. Found: C, 73.38; H, 5.49; N, 1.03; S, 2.44. IR (KBr, cm^{-1}): 3047 (w), 3023 (m), 2953 (w), 2917 (m), 2863 (w), 1608 (s), 1514 (m), 1454 (s), 1408 (m), 1384 (s), 1111 (w), 1021 (m), 857 (w), 846 (w), 832 (w), 818 (m), 800 (s), 785 (w), 767(s), 739 (m), 713 (m), 703 (m), 583 (m), 533 (s). Mp: 108−112 °C (dec).

$[Fe_2(\mu\text{-}O_2CAr^{Tol})_3(O_2CAr^{Tol})(picSPh)]$ (10). Compound **10** was recrystallized from CH_2Cl_2 layered with pentane. After 3 days, the resulting yellow needles were washed with pentane and dried at room temperature. Yield: 123 mg, 78%. X-ray diffraction quality single crystals were grown from a saturated chlorobenzene/dichloromethane solution of the complex with pentane, yielding **10**·1.5CH_2Cl_2·0.5C_6H_5Cl. Anal. Calcd for **10**·0.75CH_2Cl_2, $C_{96.75}H_{80.5}NCl_{1.5}O_8SFe_2$ (M_r = 1582.11 g/mol): C, 73.45; H, 5.13; N, 0.89; S, 2.03. Found: C, 73.32; H, 5.23; N, 0.88; S, 2.37. IR (KBr, cm^{-1}): 3053 (w), 3022 (w), 2919 (m), 2859 (m), 1603 (s), 1514 (m), 1453 (m), 1408 (m), 1384 (s), 1020 (w), 858 (w), 844 (w), 817 (m), 799 (s), 786 (w), 767 (m), 740 (m), 713 (w), 703 (w), 584 (w), 530 (m). Mp: 237−240 °C (dec).

$[Fe_2(\mu\text{-}O_2CAr^{Tol})_3(O_2CAr^{Tol})(picSPh(Me_3))]$ (11). The solution was evaporated to dryness, and the compound was recrystallized by layering a saturated chlorobenzene (5 mL) solution of the complex with pentane (5 mL). After 5 days, the resulting yellow crystals were washed with pentane and dried under high vacuum for several hours. Yield: 152 mg, 87%. X-ray diffraction quality single crystals were selected directly from the reaction vessel. Anal. Calcd for **11**·2C_6H_5Cl, $C_{111}H_{95}NCl_2O_8SFe_2$ (M_r = 1753.54 g/mol): C, 74.66; H, 5.36; N, 0.78; S, 1.80. Found: C, 74.44; H, 5.43; N, 0.80; S, 1.97. IR (KBr, cm^{-1}): 3053 (m), 3022 (m), 2918 (m), 2857 (m), 1605 (s), 1514 (m), 1453 (s), 1407 (m), 1382 (s), 1021 (m), 858 (m), 818 (s), 799 (s), 786 (m), 766 (m), 739 (m), 702 (m), 584 (m), 543 (m). Mp: 130−134 °C (dec).

$[Fe_2(\mu\text{-}O_2CAr^{Tol})_3(O_2CAr^{Tol})(picSPh(^iPr_3))]$ (12). The solution was evaporated to dryness, and compound **12** was recrystallized by layering a saturated chlorobenzene (1.5 mL) solution of the complex with pentane (3 mL). After 3 days, the resulting yellow blocks were washed with pentane and dried under high vacuum. Yield: 144 mg, 77%. X-ray diffraction quality single crystals were selected directly from the reaction vessel, yielding **12**·2C_6H_5Cl·0.5pentane. Anal. Calcd for **12**·2C_6H_5Cl, $C_{117}H_{107}NCl_2Fe_2O_8S$ (M_r = 1869.80 g/mol): C, 75.16; H, 5.77; N, 0.75; S, 1.71. Found: C, 75.21; H, 5.93; N, 0.79; S, 1.92. IR (KBr, cm^{-1}): 3049 (m), 3018 (m), 2960 (s), 2920 (m), 2865 (m), 1603 (s), 1514 (m), 1454 (m), 1408 (m), 1381 (s), 1021 (m), 858 (m), 844 (m), 818 (m), 799 (s), 785 (m), 742 (s), 714 (m), 703 (s), 585 (m), 545 (s). Mp: 225−229 °C (dec).

$[Fe_2(\mu\text{-}O_2CAr^{Ph,Xyl})_3(O_2CAr^{Ph,Xyl})(picSPh(Me_3))]$ (13). The yellow solution was stripped to dryness and recrystallized by layering a saturated chlorobenzene solution (1.5 mL) of the complex with pentane. After several days, yellow needle-shaped blocks formed, which were washed with pentane and dried under high vacuum at room temperature. Yield: 124 mg, 74%. X-ray diffraction quality single crystals were selected directly from the reaction vessel, yielding **13**·C_6H_5Cl·0.25pentane. Anal. Calcd for **13**·C_6H_5Cl, $C_{105}H_{90}NClFe_2O_8S$ (M_r = 1673.08 g/mol): C, 75.38; H, 5.42; N, 0.84; S, 1.92. Found: C, 75.14; H, 5.42; N, 0.87; S, 1.98. IR (KBr, cm^{-1}): 3058 (m), 3024 (w), 2953 (m), 2915 (m), 2858 (w), 1608 (s), 1569 (m), 1455 (w), 1438 (m), 1420 (w), 1384 (s), 1512 (w), 1021 (m), 851 (m), 811 (w), 757 (s), 700 (s), 678 (w), 625 (w), 530 (w), 488 (w). Mp: 138−142 °C (dec).

$[Fe_2(\mu\text{-}O_2CAr^{Tol})_3(O_2CAr^{Tol})(picOEt)]$ (14). Diethyl ether vapor diffusion into the yellow solution yielded yellow needles within 5 days. The crystals were washed with diethyl ether and dried at room temperature. Yield: 103 mg, 69%. X-ray diffraction quality single crystals were selected directly from the reaction vessel, yielding **14**·CH_2Cl_2·$0.75Et_2O$. Anal. Calcd for **14**·$0.5CH_2Cl_2$, $C_{92.5}H_{80}NClO_9Fe_2$ (M_r = 1496.77 g/mol): C, 74.23; H, 5.39; N, 0.94. Found: C, 74.17; H, 5.68; N, 0.92. IR (KBr, cm^{-1}): 3049 (w), 3022 (w), 2968 (w), 2918 (m), 2855 (w), 1604 (s), 1572 (w), 1543 (w), 1514 (m), 1452 (s), 1407 (w), 1383 (s), 1109 (m), 1070 (w), 1054 (w), 1021 (m), 859 (w), 842 (w), 834 (w), 818 (m), 798 (s), 768 (m), 737 (m), 714 (m), 703 (m), 584 (m), 532 (s). Mp: 135−138 °C (dec).

Physical Measurements. Elemental analyses were performed by Quantitative Technologies Inc. (QTI), Whitehouse, NJ. Melting points were determined on an Electrothermal Mel-Temp melting point apparatus. ^1H NMR spectra were measured with a Varian 300 MHz spectrometer, and VT-NMR spectra were collected by using a Varian 500 MHz spectrometer at the MIT Department of Chemistry Instrumentation Facility. Chemical shifts were referenced to residual solvent peaks. All spectra were recorded at ambient temperature. Fourier transform IR spectra were recorded on a Thermo Nicolet Avatar 360 spectrometer with the *OMNIC* software.

Mössbauer Spectroscopy. Zero-field Mössbauer spectra were recorded on an MSI spectrometer (WEB Research Co.) with an ^{57}Co source in a Rh matrix. A powdered solid diiron sample (typically 10−25 μmol or 1−2 μmol for ^{57}Fe-enriched samples) was suspended in Apiezon grease, packed into a nylon sample holder, and the spectrum was measured at 4.2 K. The isomer shift (δ) is reported with respect to that of natural iron foil used for velocity calibration. The spectra were fit with the WMOSS plot and fit program.[30]

X-ray Crystallographic Studies. Intensity data were recorded on a Bruker APEX CCD diffractometer with graphite-monochromated Mo Kα radiation ($\lambda = 0.71073$ Å) using the *SMART* software package.[31] Single crystals were mounted in Paratone N oil on the tips of glass fibers or in loops under a stream of dinitrogen maintained by a KRYO-FLEX low-temperature apparatus. Full-matrix least-squares refinement was carried out on F^2 values using the *SHELXTL* software, and empirical absorption corrections were applied with *SADABS*.[32] All non-hydrogen atoms were located and their positions were refined with anisotropic thermal parameters by successive least-squares cycles and Fourier syntheses. The hydrogen atoms were assigned to idealized positions and given thermal parameters of 1.5 (methyl hydrogens) or 1.2 (non-methyl hydrogens) times the thermal parameter of the carbon atom to which they were attached. All structures were validated by using the *PLATON* software.[33] ORTEP diagrams, atom-labeling schemes, crystal data, data collection parameters, structure refinement details, and CIF files for complexes **2**, **3**, and **5**−**14** are provided as Supporting Information.

Oxidation Product Analysis. In a typical experiment, 25 μmol of the complex were dissolved in toluene (7 mL) in an anaerobic glovebox under a dinitrogen atmosphere. Dried dioxygen was bubbled through the 3.6 mM solution for 1 min at room temperature, and the solution was stirred under a dioxygen atmosphere. After 1 h, Chelex (an ethylenediaminetetraacetic acid based solid metal ion chelator) was added, and the reaction mixture was stirred overnight. After filtration, 25 μmol of an internal standard (triptycene) were added, and the colorless solution was stripped to dryness. The remaining solid was extracted into $CDCl_3$, and the products were quantified by ^1H NMR spectroscopy. Accurate phasing, background correction, signal-to-noise ratio, and full spin−lattice relaxation (delay time between excitations ≥20 s) were accounted for in the analysis. The products were identified by comparison with authentic samples and quantified by their characteristic methylene signal (~4 ppm) and C_6 proton (~8.5 ppm) from the pyridine ring versus the bridging C−H from the triptycene standard (5.44 ppm in $CDCl_3$). Overlapping peaks in picSPh were deconvoluted with Lorentzian lines. No additional oxidation products were detected by NMR or GC/MS spectroscopy (an Agilent 6890N gas chromatograph connected to an Agilent 5973N mass spectrometer with an Agilent HP-5ms column). All measurements were within the ±5% accuracy limits expected for NMR quantification procedures.

Scheme 1. Synthetic Pathway Used To Generate Asymmetric *m*-Terphenylcarboxylate Ligands[a]

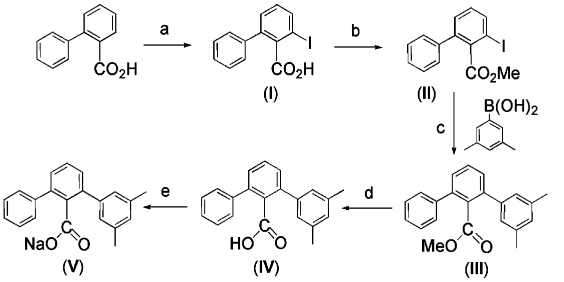

[a] (a) *s*-BuLi, THF, −78 °C, I_2, HCl (70%), ref 21; (b) MeI, Cs_2CO_3, DMF, r.t. (95%); (c) $PdCl_2(PPh_3)_2$, 1 M Na_2CO_3, THF, 60 °C (81%); (d) LiI, pyridine, 120 °C (92%); (e) NaOH, MeOH, 60 °C (quantitative).

Results and Discussion

Synthesis of the Terphenyl-Based Asymmetric Carboxylate Ligand $NaO_2CAr^{Ph,Xyl}$. The method described here for preparing of $NaO_2CAr^{Ph,Xyl}$ is a straightforward, high-yield synthetic route to asymmetric terphenyl-2′-carboxylates (Scheme 1 and Chart 2). Esterification of 3-iodobiphenyl-2-carboxylic acid with Cs_2CO_3 and methyl iodide in DMF followed by Suzuki cross-coupling of the iodide with 3,5-dimethylphenylboronic acid with 5 mol % $[PdCl_2(PPh_3)_2]$ and Na_2CO_3 in THF at 60 °C yielded $MeO_2CAr^{Ph,Xyl}$. Saponification with lithium iodide in pyridine at 120 °C followed by deprotonation of the acid with NaOH in MeOH resulted in the desired sodium salt of the asymmetric carboxylate ligand. The overall yield starting from 3-iodobiphenyl-2-carboxylic acid was 71%.

Reports on the synthesis of asymmetric *m*-terphenyl-based 2′-carboxylates are scarce. In one synthetic scheme, methyl 2,6-di-*p*-tolylbenzoate (MeO_2CAr^{Tol}) was brominated with *N*-bromosuccinimide in the presence of a catalytic amount of benzoyl peroxide in CCl_4. The resulting asymmetric terphenyl product was monobrominated at the benzylic position; however, the preparation suffers from a very low yield. The product was converted to its ester monoaldehyde via Kornblum oxidation with DMSO and sodium

---

(30) Kent, T. A. *WMOSS, Mössbauer Spectral Analysis Software*, version 2.5; WEB Research Co.: Minneapolis, MN, 1998.

(31) *SMART, Software for the CCD Detector System*, version 5.6; Bruker AXS; Madison, WI, 2000.

(32) (a) Sheldrick, G. M. *SHELXTL00: Program for Refinement of Crystal Structures*; University of Göttingen: Göttingen, Germany, 2000. (b) *SHELXTL, Program Library for Structure Solution and Molecular Graphics*, version 6.10; Bruker AXS: Madison, WI, 2001. (c) Sheldrick, G. M. *SADABS: Area-Detector Absorption Correction*; University of Göttingen: Göttingen, Germany, 2001.

(33) Spek, A. L. *PLATON, A Multipurpose Crystallographic Tool*; Utrecht University: Utrecht, The Netherlands, 2000.

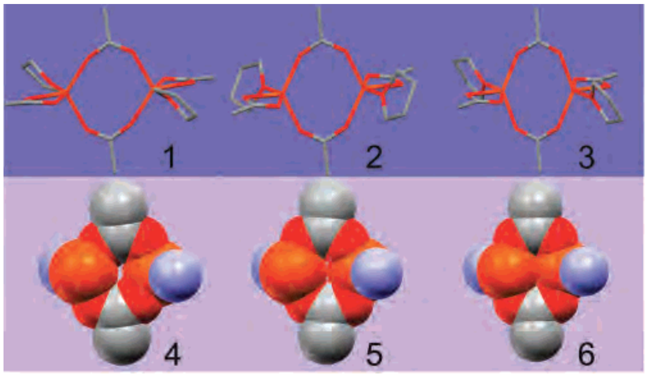

Figure 1. Graphical representation based on X-ray coordinates [capped sticks (top) and space filling (bottom)] of the contraction of the diiron core for isomeric diiron(II) complexes: **1** (top left), **2** (top middle), **3** (top right), **4** (bottom left), **5** (bottom middle), and **6** (bottom right).

bicarbonate.[34] In addition, a series of 2,6-dimethyl-1,1′:3′,1″-terphenyl-2′-carboxylates were prepared using sterically hindered esters. Reaction of 2,6-diisopropylphenyl 2,6-dimethoxybenzoate with 2,6-dimethylphenyl or mesityl Grignard reagents (2,6-$Me_2PhMgBr$ and 2,4,6-$Me_3PhMgBr$) afforded the monoarylated products, which were then converted into a terphenyl with less sterically demanding aryl Grignard reagents (PhMgBr and 3,5-Me_2PhBr).[35] The $^-O_2CAr^{Ph,Xyl}$ carboxylate is not accessible by this route because it requires a bulky 2,6-xylyl moiety on one of the terphenyl arms.[35] Therefore, the two synthetic strategies are complementary, allowing the preparation of a variety of asymmetric terphenylcarboxylates.

Preparation and Crystallographic Analysis of 2, 3, 5, and 6. Complexes **2** and **3** were prepared in THF by reacting $Fe(OTf)_2{\cdot}2MeCN$ with NaO_2CAr^{Tol} and $NaO_2CAr^{Ph,Xyl}$ in a 1:1:1 ratio or mixing $Fe(OTf)_2{\cdot}2MeCN$ and $NaO_2CAr^{Ph,Xyl}$ in a 1:2 ratio, respectively, in a manner similar to that in previously reported procedures.[6,7] Recrystallization from CH_2Cl_2 by pentane vapor diffusion resulted in colorless crystals in good to moderate yield (64 and 48% for **2** and **3**, respectively). All of our attempts to prepare complexes with mixed carboxylates in a 1:3 or 3:1 ratio failed, and only crystals containing either the carboxylates in 1:1 stoichiometry or only the $^-O_2CAr^{Tol}$ carboxylate could be isolated and analyzed by X-ray diffraction. Complexes containing the symmetric carboxylate are less soluble than those of its asymmetric analogue. Compounds **5** and **6** were prepared by displacement of THF in **2** and **3** by pyridine in CH_2Cl_2. Crystallization of the products from CH_2Cl_2/pentane or toluene/pentane resulted in yellow blocks in good yield (53 and 89%, respectively).

The structural features of **2**, **3**, **5**, and **6** were compared with those of the corresponding complexes containing only 2,6-di-*p*-tolylbenzoate carboxylate ligands, $[Fe_2(\mu\text{-}O_2CAr^{Tol})_2(O_2CAr^{Tol})_2(THF)_2]$ (**1**) and $[Fe_2(\mu\text{-}O_2CAr^{Tol})_2(O_2CAr^{Tol})_2(pyridine)_2]$ (**4**). The diiron cores of **1**−**6** are depicted in Figure 1. Selected interatomic distances and angles are given in Table 1. The most striking feature in this series of isomeric complexes is the large variation in the Fe−Fe distance, which depends on the identity of the carboxylate ligand. For both the THF- and pyridine-containing complexes, increasing the asymmetry of the carboxylates significantly decreases the metal−metal separation. The diiron distance reduces from 4.2822(7) (**1**) to 3.6598(8) Å (**3**) for the THF series and from 4.2189(13) (**4**) to 3.355[10][36] Å (**6**) for the pyridine complexes (Table 1). The Fe−Fe distances are inversely correlated with the O(1)−Fe(1)−O(2) angles, which are 114.33(9)° and 116.42(13)° in **1** and **4**, respectively, and 133.54(8)° and 144.96[19]° in **3** and **6**, respectively. The Fe−O−C angles decrease with a shortening of the diiron distance and an increase in the O−Fe−O angles. The correlations of the diiron core distances with the O−Fe−O and Fe−O−C angles for **1**−**6** as well as for additional examples from the literature are illustrated in Figure 2. The Fe−N (2.143(3) and 2.114[2] Å in **5** and **6**, respectively) and Fe−O (1.957(3)−2.358(3) Å in **2**, **3**, **5**, and **6**) distances do not exhibit any unexpected features and are comparable to those in **1** and **4**.[6]

The ability to control the Fe−Fe distance in carboxylate-bridged dinuclear complexes in the manner just described is interesting in the context of a recent computational quantum mechanics/molecular mechanics analysis of the diiron core in $MMOH_{red}$. This work revealed that the protein matrix compresses the active site, thereby destabilizing intermediates that lie closer to the reduced form of the enzyme and facilitating the formation of the methane-oxidizing diiron(IV) species Q.[37] The shortening of the metal−metal distance facilitates the formation of a μ-1,1-monobridged species (Chart 1). Oxidation reactions of a series of diiron(II) complexes containing the dinucleating ligand *N*,*N*,*N*′,*N*′-tetrakis(2-pyridylmethyl)-2-hydroxy-1,3-diaminopropane (HPTP), which features a bridging alkoxo group with one or two supporting phenylcarboxylate bridges, reveal that complexes with one bridging carboxylate form a peroxo intermediate 1 order of magnitude more rapidly than a dicarboxylate-bridged analogue does.[38] In addition, the peroxo intermediate of $[Fe^{II}_2(HPTP)(\mu\text{-}O_2CC_6H_5)](BPh_4)_2$ converts phosphines, sulfides, and alcohols to their oxidation products, whereas reaction of the corresponding $[Fe^{II}_2(HPTP)(\mu\text{-}O_2CC_6H_5)_2](BPh_4)$ complex did not result in the formation of any oxidation products.[38]

Windmill complexes having short iron−iron distances were previously thought to be difficult to synthesize in the absence of external compression, such as from a protein matrix, with the reported Fe−Fe vectors being between 3.96 and 4.22 Å in length.[3] Recently, we found that, by using 2,6-bis(3,5-dimethylphenyl)benzoate ($^-O_2CAr^{Xyl}$), we could assemble synthetic model complexes with diiron distances

---

[34] Farrell, J. R.; Stiles, D.; Bu, W.; Lippard, S. J. *Tetrahedron* **2003**, *59*, 2463−2469.

[35] Hattori, T.; Koshiishi, E.; Wada, S.; Koike, N.; Yamabe, O.; Miyano, S. *Chirality* **1998**, *10*, 619−626.

[36] Parentheses refer to unique values and square brackets to average values calculated by the following equations. Considering a sample of n observations x_i, the unweighted mean value (x_u) with its standard deviation (σ) was calculated using the following equations: $x_u = \sum_i x_i/n$; $\sigma = \{\sum_i (x_i - x_u)^2/[n(n-1)]\}^{1/2}$.

[37] Rinaldo, D.; Philipp, D. M.; Lippard, S. J.; Friesner, R. A. *J. Am. Chem. Soc.* **2007**, *129*, 3135−3147.

[38] Costas, M.; Cady, C. W.; Kryatov, S. V.; Ray, M.; Ryan, M. J.; Rybak-Akimova, E. V.; Que, L., Jr. *Inorg. Chem.* **2003**, *42*, 7519−7530.

Table 1. Selected Interatomic Distances (Å) and Angles (deg) for **1**−**6**

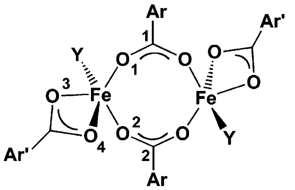

	$\mathbf{1}\cdot 2CH_2Cl_2$[a]	$\mathbf{2}\cdot 2CH_2Cl_2$	$\mathbf{3}\cdot 0.5CH_2Cl_2$	**4**[a]	$\mathbf{5}\cdot 4CH_2Cl_2$	**6**
			Atom 1−Atom 2 (Å)			
Fe−Fe	4.2822(7)	4.0248(10)	3.6598(8)	4.2189(13)	3.9851(15)	3.355[10][b]
Fe−O1	1.9428(19)	1.979(2)	1.9583(19)	2.006(3)	1.958(2)	1.992[4]
Fe−O2	2.0061(18)	1.975(2)	2.0143(19)	1.957(3)	2.021(2)	1.981[4]
Fe−O3	2.0363(19)	2.051(2)	2.054(2)	2.047(3)	2.073(2)	2.064[3]
Fe−O4	2.3455(19)	2.271(2)	2.259(2)	2.358(3)	2.310(2)	2.294[11]
Fe−Y	2.0941(19)	2.090(2)	2.090(2)	2.132(4)	2.143(3)	2.114[2]
			Atom 1−Atom 2−Atom 3 (deg)			
O1−Fe1−O2	114.33(9)	123.05(11)	133.54(8)	116.42(13)	125.35(11)	144.96[19]
Fe1−O1−C1	156.64(19)	145.7(2)	141.03(18)	152.8(3)	147.6(2)	134.4[1]
Fe1−O2−C2	135.98(18)	138.4(2)	130.80(18)	135.6(3)	135.6(2)	131.2[2]
Fe1−O−C[c]	146.3	142.1	135.9	144.2	141.6	133.1

[a] Data from ref 6. [b] Parentheses refer to unique values and square brackets to average values calculated by the equations shown in ref 36. [c] Average value for Fe1−O1−C1 and Fe1−O2−C2.

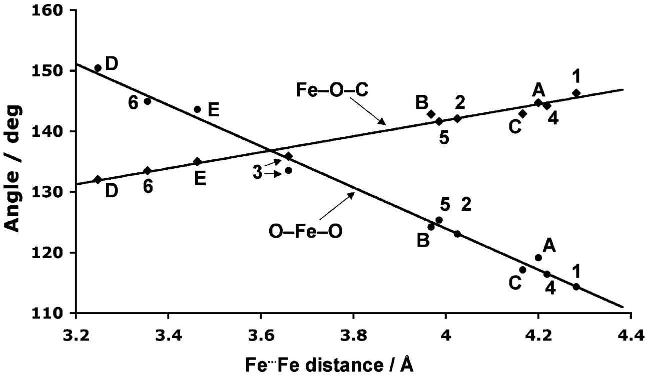

Figure 2. Correlation between Fe−Fe distances and Fe−O−C and O−Fe−O angles for the bridging carboxylates in the windmill complexes **1**−**6** (Table 1): $[Fe_2(\mu\text{-}O_2CAr^{Tol})_2(O_2CAr^{Tol})_2(MeIm)_2]$ (A) Fe−Fe = 4.200[3] Å, O−Fe−O = 119.14[40]°, Fe−O−C = 144.7°;[6] $[Fe_2(\mu\text{-}O_2CAr^{Tol})_2(O_2CAr^{Tol})_2(MeCN)_2]$ (B) Fe−Fe = 3.968[8] Å, O−Fe−O = 124.2[3]°, Fe−O−C = 142.8°;[7] $[Fe_2(\mu\text{-}O_2CAr^{4-FPh})_2(O_2CAr^{4-FPh})_2(THF)_2]$ (C) Fe−Fe = 4.17[2] Å, O−Fe−O = 117.1[5]°, Fe−O−C = 142.9°;[7] $[Fe_2(\mu\text{-}O_2CAr^{Xyl})_2(O_2CAr^{Xyl})_2(NH_2(CH_2)_3SCH_3)_2]$ (D) Fe−Fe = 3.2475(8) Å, O−Fe−O = 150.43°, Fe−O−C = 132.0°;[19] $[Fe_2(\mu\text{-}O_2CAr^{Xyl})_2(O_2CAr^{Xyl})_2(NH_2(CH_2)_3CCH)_2]$ (E) Fe−Fe = 3.4629(17) Å, O−Fe−O = 143.46°, Fe−O−C = 135.0°.[19]

similar to that in $MMOH_{red}$, with the particular examples being $[Fe_2(\mu\text{-}O_2CAr^{Xyl})_2(O_2CAr^{Xyl})_2(NH_2(CH_2)_3SCH_3)_2]$, [Fe−Fe] 3.2475(8) Å, and $[Fe_2(\mu\text{-}O_2CAr^{Xyl})_2(O_2CAr^{Xyl})_2(NH_2(CH_2)_3CCH)_2]$, [Fe−Fe] 3.4629(17) Å.[19]

By designing the asymmetric carboxylate $^{-}O_2CAr^{Ph,Xyl}$, we intended in the present work to improve our chances of synthesizing an $MMOH_{red}$ model complex having a short Fe−Fe distance as well as a monoatom bridging motif, with either mixed symmetric and asymmetric carboxylate ligands or only the latter. Although we were unable to prepare complexes with symmetric ($^{-}O_2CAr^{Tol}$) and asymmetric ($^{-}O_2CAr^{Ph,Xyl}$) carboxylates having a 1:3 or 3:1 ratio, we succeeded in isolating such complexes in 1:1 stoichiometry as well as windmill complexes containing the purely asymmetric carboxylate ligand. Even without a monoatom-bridged carboxylate, the diiron(II) centers in complexes **3** and **6** are compressed to an extent similar to that observed in $MMOH_{red}$. Although crystal lattice forces cannot be excluded, we conclude that the sterically less demanding *o*-xylyl-substituted benzoates are responsible for this shortening, which is not encountered in the more commonly employed 2,6-di-*p*-tolylbenzoate ligands. A structural comparison of **2** and **5**, versus **3** and **6**, reveals the influence of the carboxylate ligands on the core geometry and identifies the bridging ligand as being responsible for preventing compression of the diiron center (Table 1). Replacement of the terminal $^{-}O_2CAr^{Tol}$ by $^{-}O_2CAr^{Ph,Xyl}$ in **2** and **5** results in only a moderate diiron distance shortening of ~0.25 Å, whereas replacement of the bridging carboxylate decreases the corresponding distance by 0.37 and 0.63 Å in **3** and **6**, respectively. The X-ray structures of complexes **1** and **4** reveal repulsion between the methyl groups of the tolyl arms of the two bridging carboxylates ($H_3C\cdots CH_3$ = 3.863 and 4.073 Å, respectively). These groups interact across the diiron center and keep the two metal atoms from approaching one another more closely. In diiron(II) windmill complexes with $^{-}O_2CAr^{Ph,Xyl}$ and $^{-}O_2CAr^{Xyl}$ ligands, no such intramolecular repulsion is observed.

Synthesis and Structural Characterization of Diiron(II) Complexes 7−14. Both the more commonly used $^{-}O_2CAr^{Tol}$ and the asymmetric $^{-}O_2CAr^{Ph,Xyl}$ carboxylate ligands were employed to prepare diiron(II) complexes with appended substrates in order to evaluate their influence on structural features and oxidation properties in comparison with previous work. The reaction of $[Fe_2(\mu\text{-}O_2CAr)_2(O_2CAr)_2(THF)_2]$ (**1**, Ar = Ar^{Tol} or $Ar^{Ph,Xyl}$) with 1.2 equiv of a pyridine ligand bearing a tethered substrate resulted in a shift of one of the bridging *m*-terphenylcarboxylate ligands to a terminal bidentate mode with displacement of both THF ligands, affording the neutral and triply bridged diiron(II) complexes **7**−**14** (Scheme 2). Use of excess substrates (up

Scheme 2. (a) Synthesis of Picolyl-Based Thioethers (picSR), (b) General Procedure for the Preparation of the Diiron(II) Compounds **7**−**13**, and (c) Dioxygen Oxidation of the Tethered Substrates to the Corresponding Sulfoxides

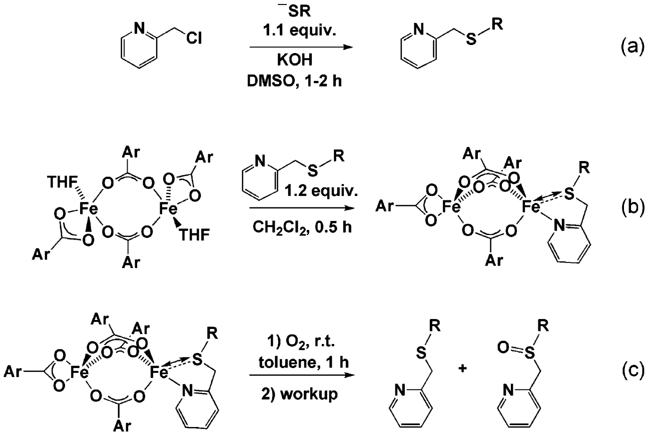

to 3 equiv) resulted in the formation of the same compounds, and a complex with two pyridine ligands was not isolated in any case. The structures of **7**−**14** were determined by X-ray diffraction and are depicted for **10**−**12** in Figure 3. ORTEP drawings with atom-labeling schemes for the other compounds can be found in the Supporting Information. Selected interatomic distances and angles are given in Table 2. All complexes contain a triply bridged diiron(II) core with one additional *m*-terphenyl-based carboxylate ligand, coordinated to the Fe(2) center, completing a distorted trigonal-bipyrimidal coordination sphere for the latter. The diiron distances of ∼3.4 Å are comparable to that in MMOH$_{\mathrm{red}}$, ∼3.3 Å.[39] The coordination sphere of Fe(1) contains an additional picolyl-based thioether group, which binds to the metal center to form a five-membered chelate ring (**7**−**10**) or as a monodentate ligand via the nitrogen atom (**11**−**13**), depending on the steric properties of the appended sulfide. In particular, the coordination geometry at Fe(1) switches from distorted trigonal bipyramidal with an NSO_3 donor set in **7**−**10** to distorted tetrahedral with an NO_3 donor set in **11**−**13**. We were particularly interested in increasing the Fe···S distance to investigate whether C−H bond activation rather than sulfoxidation might be induced as a consequence of these steric modifications of R in picSR. The mesityl and triisopropyl substituents are sufficiently bulky (Figure 3) to push the sulfur atom away from the iron center, possibly favoring oxidation of the methylene instead of the thioether group (see below).

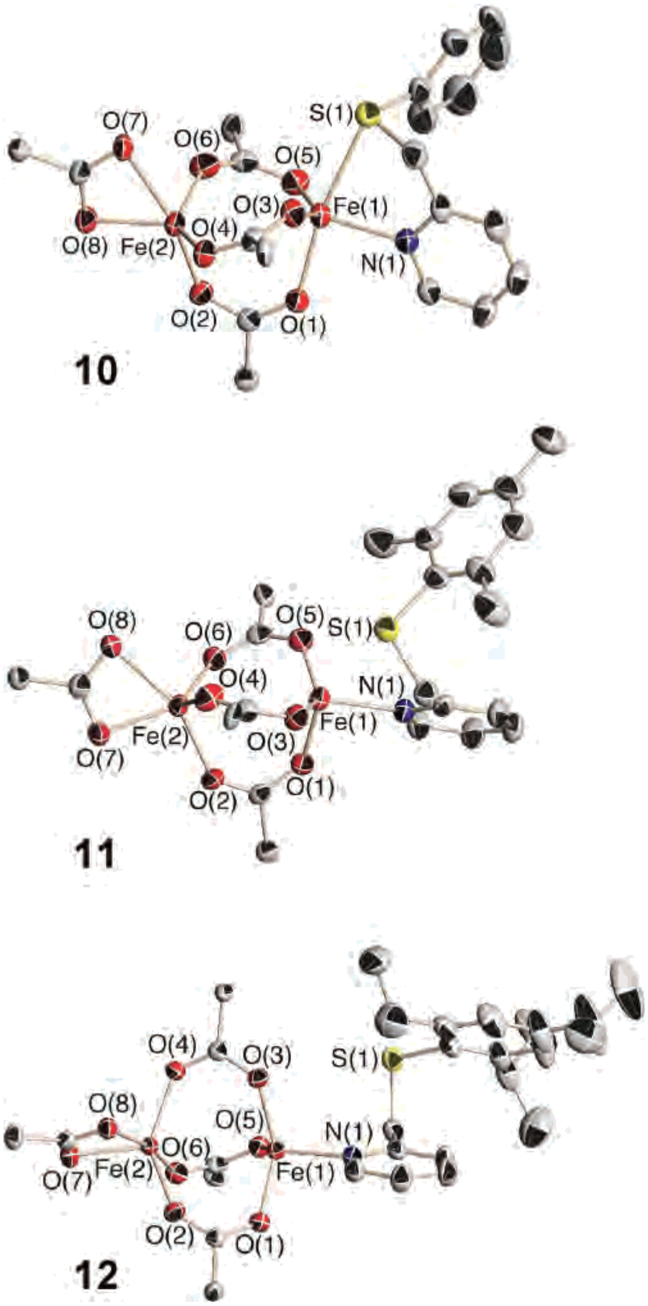

Figure 3. Molecular structures of **10** (top), **11** (middle), and **12** (bottom) showing 50% probability thermal ellipsoids and the atom-numbering scheme for all non-carbon atoms. The aromatic rings of carboxylate ligands, hydrogen atoms, and lattice molecules are omitted for clarity.

The average Fe(1)−Fe(2) distance for high-spin complexes with the $\{Fe_2(\mu\text{-}O_2CAr^{Tol})_2(O_2CAr^{Tol})_2(\text{picSR})\}$ core in **7**−**12** is 3.36[5][36] Å. This value falls between those of windmill complexes and paddlewheel compounds and is typical for triply carboxylate-bridged diiron(II) centers.[7,17] The iron−iron distance in **13**, which incorporates the asymmetric carboxylate ligand $^{-}O_2CAr^{Ph,Xyl}$, is significantly longer than those in **7**−**12**, which have the $^{-}O_2CAr^{Tol}$ ligand. The corresponding distance in **6** is comparable to the values in **7**−**12** but is significantly shorter than the one observed in **13**, unexpectedly causing the diiron distance in the triply bridged complex **13** to be longer than that in the windmill complex **6**. The Fe(1)−N(1) bond length varies only marginally [2.085(2)−2.128(3) Å] throughout compounds **7**−**14** and agrees with previously reported Fe^{II}−N(pyridine) bond lengths.[17] As anticipated, the Fe(1)−thioether bond distances differ considerably when the different thioethers are employed. The long Fe^{II}−S bond lengths in **7**−**10** [Fe(1)−S(1) = 2.6024(9)−2.6575(18) Å] are indicative of weakly coordinated sulfur and are comparable to the reported value of 2.572(1) Å in the high-spin iron(II) thioether complex [Fe^{II}(“$N_2H_2S_3$”)]$_2$ [“$N_2H_2S_3$”H_2 = 2,2′-bis[(2-mercaptophenyl)-

---

(39) Whittington, D. A.; Lippard, S. J. *J. Am. Chem. Soc.* **2001**, *123*, 827−838.

Table 2. Selected Interatomic Distances (Å) and Angles (deg) for **7**−**14**

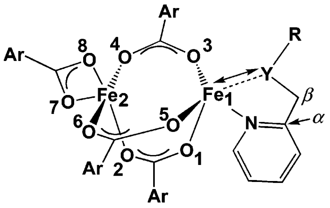

	7	**8**	**9**	**10**	**11**	**12**	**13**	**14**
				Atom 1−Atom 2 (Å)				
Fe1−Fe2	3.3494(6)	3.3054(7)	3.4664(6)	3.3370(11)	3.4659(8)	3.2284(5)	3.5531(24)	3.3631(6)
Fe1−Y	2.6120(9)	2.6168(11)	2.6024(9)	2.6575(18)	3.1984(14)	4.0258(8)	2.8174(31)	2.297(2)
Fe1−N	2.128(3)	2.121(3)	2.116(2)	2.114(5)	2.106(3)	2.085(2)	2.123(4)	2.098(2)
Fe1−O1	2.075(2)	2.071(2)	2.068(2)	2.066(4)	2.028(3)	1.9889(18)	2.061(4)	2.0701(19)
Fe1−O3	2.009(2)	2.001(2)	1.985(2)	2.006(4)	1.975(3)	1.9891(17)	1.990(4)	1.9987(19)
Fe1−O5	2.011(2)	2.026(2)	2.015(2)	2.005(4)	1.997(3)	1.9753(18)	1.980(3)	1.9996(19)
Fe2−O2	2.033(2)	2.029(2)	2.020(2)	2.029(4)	2.035(3)	2.0232(18)	2.046(3)	2.0287(19)
Fe2−O4	2.042(2)	2.054(2)	2.023(2)	2.019(4)	2.025(3)	2.0409(17)	2.063(3)	2.0521(19)
Fe2−O6	2.051(2)	2.035(2)	2.032(2)	2.018(4)	2.018(3)	2.0519(18)	2.045(3)	2.0298(19)
Fe2−O7	2.065(2)	2.055(2)	2.184(3)	2.055(4)	2.066(3)	2.0598(17)	2.070(3)	2.0588(19)
Fe2−O8	2.258(2)	2.253(2)	2.166(3)	2.275(4)	2.249(3)	2.2573(18)	2.344(4)	2.262(2)
				Atom 1−Atom 2−Atom 3 (deg)				
N−Fe1−Y	77.46(8)	79.04(9)	79.47(7)	78.42(13)	71.64(10)	59.03(6)	76.09(11)	74.02(9)
O1−Fe1−Y	167.35(6)	170.25(7)	168.00(6)	169.69(12)	156.30(9)	142.94(5)	163.70(9)	164.60(8)
O1−Fe1−N	90.06(9)	91.21(11)	88.70(9)	91.36(17)	89.78(13)	90.86(8)	88.91(14)	91.29(9)
O3−Fe1−Y	86.11(6)	82.65(6)	91.50(7)	81.05(12)	100.30(9)	75.36(5)	108.12(6)	81.49(8)
O3−Fe1−N	100.48(9)	96.45(11)	106.93(10)	95.00(17)	102.96(13)	99.55(8)	98.42(14)	102.93(9)
O5−Fe1−Y	88.35(6)	87.56(7)	81.28(7)	91.59(13)	68.49(9)	77.44(5)	95.73(10)	90.52(8)
O5−Fe1−N	117.09(9)	117.05(11)	111.78(10)	124.47(17)	113.06(13)	123.63(8)	131.66(15)	115.52(9)
				Atom 1−Atom 2−Atom 3−Atom 4 (deg)				
N−C_α−C_β−Y	44.58(35)	40.85(48)	38.88(39)	38.25(71)	59.66(48)	87.14(25)	47.39(53)	33.66(39)

amino]diethyl sulfide].[40] The isolation and structural characterization of complex **14**, in which the sulfur atom is replaced by oxygen, displays Fe−O bond lengths of 2.297(2) Å. This result is consistent with the weak coordination of the sulfur atom in **7**−**10** because the alkyl chains in the substrates have little steric restraint and are thus not responsible for elongating the iron−heteroatom bonds. However, replacement of the alkyl or phenyl substituents in **7**−**10** by the sterically more demanding mesityl (**11** and **13**) or 2,4,6-triisopropylphenyl (**12**) group has a considerable influence on coordination to Fe(1), resulting in a distorted tetrahedral environment, with no Fe−S bond occurring in **11**−**13**. In these compounds, the distances are Fe(1)−S(1) = 3.1984(14), 4.0258(8), and 2.8174(31) Å, respectively. The Fe⋯S distances for the previously reported compounds [$Fe_2(\mu\text{-}O_2CAr^{Tol})_3(O_2CAr^{Tol})$(pySR)] are 2.909 Å (R = Me), and 3.090 Å (R = Ph).[17] The sulfur atom of the picSPh(Me_3) ligand is closer to the diiron center in **13**, which employs four 3,5-dimethyl-1,1′:3′,1″-terphenyl-2′-carboxylates, than in **11**, which contains the 2,6-di-*p*-tolylbenzoate ligands. Therefore, the iron−sulfur separation can be tuned both by variation of the steric bulk at the tethered substrates and independently by the choice of the carboxylate ligands. Correlations between the iron−sulfur distance, the N−Fe−S bond angle, and the N−C_α−C_β−S dihedral angle are depicted in Figure 4, which reveals that an increasing Fe−S distance reflects a smaller N−Fe−S bond angle and a larger torsion angle.

Table 3. Mössbauer Parameters (δ, ΔE_Q, and Γ) for Compounds **10**−**12**

compound	δ/mm s^{-1}	ΔE_Q/mm s^{-1}	Γ/mm s^{-1}
10	1.17(2)	2.91(2)	0.34(2)
11, Fe(1)	1.16(2)	2.45(2)	0.33(2)
11, Fe(2)	1.22(2)	2.95(2)	0.30(2)
12, Fe(1)	1.05(2)	2.23(2)	0.31(2)
12, Fe(2)	1.20(2)	2.79(2)	0.29(2)

Evidence that the distinct structural changes manifested by **10**−**12** in the solid state may prevail in solution derives from optical spectroscopic measurements. Compound **12** in CH_2Cl_2 exhibits a weak ($\epsilon \sim 300$ M^{-1} cm^{-1}) absorption band at 1018 nm that is absent in the spectrum of **10**. We tentatively attribute the presence of this low-energy feature to structural alterations induced by the sterically demanding picSPh(^{i}Pr)$_3$ substrate in **12**.

Mössbauer Spectroscopy. Figure 5 displays the Mössbauer spectra for compounds **10**−**12**, and the derived parameters are reported in Table 3. At zero field and 4.2 K, the Mössbauer parameters are typical of high-spin iron(II) complexes having a carboxylate-rich coordination environment.[3,41] The spectrum of compound **10** (δ = 1.17(2) mm

---

(40) Sellmann, D.; Utz, J.; Heinemann, F. W. *Inorg. Chem.* **1999**, *38*, 459−466.

(41) (a) Kurtz, D. M., Jr. *Chem. Rev.* **1990**, *90*, 585−606. (b) Gütlich, P.; Ensling, J. In *Inorganic Electronic Structure and Spectroscopy*; Solomon, E. I., Lever, A. B. P., Eds.; Wiley: New York, 1999; Vol. 1, pp 161−211. (c) Münck, E. In *Physical Methods in Bioinorganic Chemistry: Spectroscopy and Magnetism*; Que, L., Jr., Ed.; University Science Books: Sausalito, CA, 2000; pp 287−319.

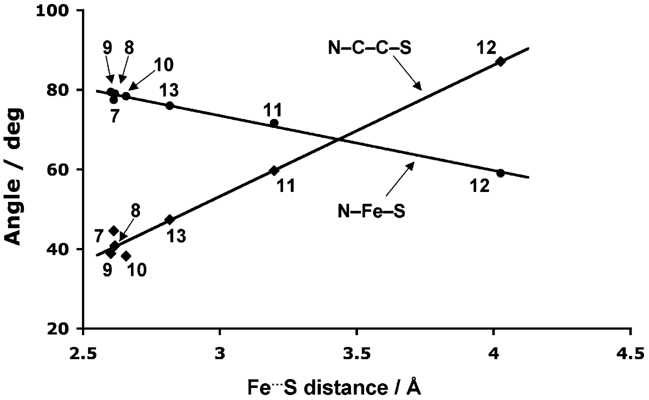

Figure 4. Correlation between the Fe···S distance, the N−Fe−S angle, and the N−C_α−C_β−S torsion angle in compounds **7**−**13**.

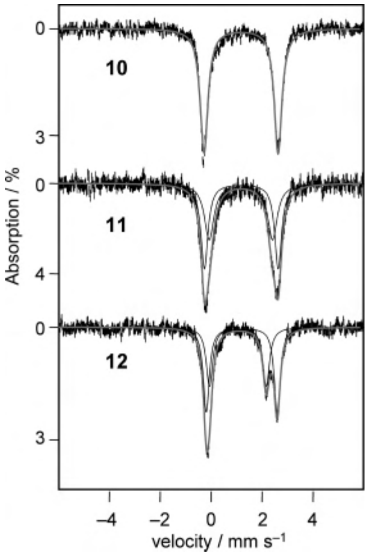

Figure 5. Zero-field Mössbauer spectra recorded at 4.2 K: **10** (top), **11** (middle), and **12** (bottom). Solid gray lines were fitted by the parameters defined in Table 3. For **11** and **12**, the fits for single quadruple splittings are also assigned (thin black lines).

s^{-1}, $\Delta E_Q = 2.91(2)$ mm s^{-1}) consists of a single sharp quadrupole doublet with $\Gamma = 0.34(2)$ mm s^{-1}, indicating that the two iron atoms have similar coordination geometries. The line width is very narrow and close to that of the natural value. Similar Mössbauer parameters and indistinguishable iron sites were reported for the diiron complex $[Fe^{II}_2(\mu\text{-}O_2CAr^{Tol})_3(O_2CAr^{Tol})(pyPPh_2)]$ ($\delta = 1.22(2)$ mm s^{-1}, $\Delta E_Q = 2.66(2)$ mm s^{-1}).[17] In agreement with this finding, the X-ray crystal structure of **10** reveals that the iron(II) atoms have similar distorted trigonal-bipyramidal coordination environments, differing only in the identity of the terminally bound ligand, a bidentate carboxylate on Fe(2), and a chelating pyridine−thioether on Fe(1) (Figure 3).

In contrast, the Mössbauer spectrum of **11** displays an absorption that is asymmetric and significantly broadened, with Γ being 0.44 mm s^{-1} when the spectrum was fit as a single quadrupole doublet. The two iron sites are distinguishable and can be deconvoluted by fitting with two quadrupole doublets, yielding the parameters in Table 3. The 4.2 K zero-field Mössbauer spectrum of complex **12** displays two overlapping quadrupole doublets with similar intensities (integration ratio = 1:1). Deconvolution results are also available in the table. Similar spectroscopic features have been reported previously for $[Fe_2(\mu\text{-}O_2CAr^{Tol})_3(O_2CAr^{Tol})(2,6\text{-lutidine})]$ ($\delta_1 = 1.05(2)$ mm s^{-1}, $\Delta E_Q = 2.18(2)$ mm s^{-1}; $\delta_2 = 1.23(2)$ mm s^{-1}, $\Delta E_Q = 2.80(2)$ mm s^{-1}). This complex has two distinct iron sites within the dinuclear unit, four-coordinate Fe(1) and five-coordinate Fe(2).[42] The isomer shift δ_2 assigned to Fe(2) does not vary significantly for complexes **10**−**12**. The coordination environment of Fe(1) differs among the complexes under study here and switches from distorted trigonal-bipyramidal geometry to distorted tetrahedral geometry from **10** to **12** (Figure 3), resulting in two distinguishable high-spin iron(II) centers in **11** and **12**. The negatively shifted δ_1 for Fe(1) in **11** and **12** agrees with a decrease in the coordination number and an increase in the expectation value $|\Psi_s(0)_s|^2$ for the s-electron density at the nucleus.[43]

Table 4. Oxidation Product Analysis Following Exposure of Compounds **10**−**13** with Dioxygen in Toluene at Room Temperature for 1 h

compound	recovered thioether[a] (%)	recovered sulfoxide[a] (%)	ratio sulfoxide/ sulfide	Fe···S (Å)
none[b]	88	0	N/A	
$Zn(OTf)_2$[b]	89	0	N/A	
$Fe(OTf)_2$[b]	88	0	N/A	
6[b]	85	0	N/A	
10[c]	19	66	3.47	2.6575(18)
11	36	55	1.53	3.1984(14)
12	40	38	0.95	4.0258(8)
13	18	63	3.50	2.8174(31)

[a] Confidence level ± 5% based on NMR quantification and reproducibility of the oxidations. [b] Performed in toluene (for **6** and when no metal was present), methanol (for $Zn(OTf)_2$), or acetonitrile (for $Fe(OTf)_2$) because of the insolubility of the metal salts in toluene. A total of 2 equiv of the metal salts and 1 equiv of **6** were used per picSPh($^iPr_3$) substrate. [c] The addition of 200 μL of MeCN did not change the oxidation chemistry of this compound.

Oxidation of Tethered Thioether Substrates. The reactions of compounds **10**−**13** with dioxygen were investigated. The complexes contain tethered substrates picSR with differing steric hindrance provided by the substituents R, resulting in variable iron−sulfur distances, which affect the ability of the thioether moiety to be oxidized. In addition, the reactivity is influenced by the choice of symmetric $^-O_2CAr^{Tol}$ compared to the asymmetric $^-O_2CAr^{Ph,Xyl}$ carboxylate ligand. The results of oxidation of the tethered substrates appended to the diiron(II) center in **10**−**13** are summarized in Table 4. The substrates were chosen for their potential ability to undergo C−H bond activation as well as sulfoxidation. Both C−H bond activation and sulfoxidation have been observed in the oxidation of various alkanes and sulfides by sMMO.[12]

When dioxygen is bubbled through a 3.6 mM solution of the diiron complexes in toluene at room temperature, the color immediately turns from yellow to brown. The reaction products formed are picS(O)Ph (**10**), picS(O)Ph(Me_3) (**11** and **13**), and picS(O)Ph($^iPr_3$) (**12**), as identified by comparison with authentic samples and quantified by ^1H NMR

---

(42) Lee, D.; Lippard, S. J. *Inorg. Chim. Acta* **2002**, *341*, 1−11.

(43) Yoon, S.; Lippard, S. J. *J. Am. Chem. Soc.* **2005**, *127*, 8386−8397.

spectroscopy (Scheme 2). The products result from sulfoxidation rather than alkane oxidation. The sulfoxides were isolated in 66, 55, 38, and 63% yields for complexes **10**−**13**, respectively, and the unoxidized picoline−thioether ligand was recovered in 19, 36, 40, and 18% yields. The observed sulfoxide/thioether ratios upon oxygenation of **10**−**13** are 3.47, 1.53, 0.95, and 3.50, respectively (Table 4). No oxidation of the thioether ligands occurs in the presence of zinc(II) or iron(II) triflate (2 equiv) in MeOH and MeCN, respectively, under similar experimental conditions. Therefore, metal-mediated oxidation based on the Lewis acid character of metal salts can be excluded, and simple iron(II) salts cannot convert the substrates to the corresponding sulfoxides. The addition of 200 μL of MeCN to a toluene solution of **10** prior to exposing the solution to dioxygen did not significantly alter the formation of oxidized products. The results indicate that the diiron(II) complexes **10**−**13** mimic aspects of the reactivity of MMOH.

We were interested in examining the importance of proximity to the diiron center for thioether oxidation. Previous work demonstrated that phosphine oxidation in $pyPPh_2$ only occurs when the substrate is attached to the pyridine donor in the ortho position.[16] In the present study, we positioned the sulfur atom in a systematic manner increasingly far from the diiron center by tethering a $-CH_2SAr$ moiety in the ortho position of a pyridine donor and varying the steric bulk in picSAr from Ar = Ph to $Ph(Me_3)$ to $Ph(^iPr_3)$ (Table 4). The yield of oxidized product, and the corresponding sulfoxide/sulfide ratio, decreases with increasing Fe···S distance. By lengthening the iron−sulfur distance, we also increased the probability for C−H bond activation of the methylene group in competition with sulfur oxidation. Increasing the iron−sulfur distance also increases the $S-C_\alpha-C_\beta-N$ torsion angle (Figure 4), thereby diminishing the Fe···H(CH) distance from 3.34 Å in **10** to 2.78 Å in **12**. This decrease would facilitate hydrogen atom abstraction at the methylene position by an oxygenated intermediate. In **12**, the Fe···S and Fe···C(methylene) distances are 4.0258(8) and 3.311(3) Å, respectively. Although these structural changes would increase the probability for C−H bond activation, allowing for at least partial methylene hydroxylation, reactivity at sulfur dominates the oxidation process, presumably for energetic reasons. No alcohols or ketones were detected in the products by GC/MS and ^{1}H NMR spectroscopic analyses.

By comparing the Fe−S distances in the alkyl sulfide derivatives **7**−**9** with that in **10**, which contains the sterically least demanding aryl sulfide, we note a much less dramatic trend (Figure 4). We therefore did not quantitate the extent of sulfoxidation in **7**−**9**. Qualitative studies indicated, however, that they do form sulfoxides under conditions similar to those applied in our investigation of **10**−**13**.

We also studied the oxidation of external substrates with **6** and the recently reported complex $[Fe_2(\mu\text{-}O_2Cbiph)_4(1\text{-}MeIm)_2]$.[9] No oxidation products were observed upon bubbling dioxygen through a toluene solution of MeSPh in the presence of $[Fe_2(\mu\text{-}O_2Cbiph)_4(1\text{-}MeIm)_2]$ or **6**. Compound **6** also did not promote the oxidation of externally added $picSPh(^iPr_3)$, indicating that the pyridine ligand is not replaced by the picoline-based substrate and that coordination of the substrate to the iron center is crucial for its oxidation. These complexes were chosen because **6** has a short iron−iron distance, which could facilitate the formation of a high-valent oxygenated intermediate, and the paddlewheel complex $[Fe_2(\mu\text{-}O_2Cbiph)_4(1\text{-}MeIm)_2]$ has sterically less hindered biphenylcarboxylates, which were introduced to facilitate access of external substrates to the active center.

Conclusion

The present study demonstrates the influence of intramolecular stereochemical interactions on the diiron core composition and sulfoxidation chemistry of carboxylate-bridged diiron(II) complexes. The preparation of the new asymmetric carboxylate ligand $^-O_2CAr^{Ph,Xyl}$ facilitates synthetic access to diiron(II) windmill complexes **2**, **3**, **5**, and **6** with variable iron−iron distances. For the first time, diiron(II) windmill complexes with mixed carboxylates could be isolated. These compounds have a 1:1:1 $Fe^{2+}/^-O_2CAr^{Ph,Xyl}/^-O_2CAr^{Tol}$ stoichiometric ratio and reveal that the bridging 2,6-di-*p*-tolylbenzoate ligands are mainly responsible for preventing the shortening of the Fe−Fe separation in **1**, **2**, **4**, and **5**. The asymmetric carboxylate ligand was also applied to assemble the triply bridged complex **13** by incorporating the tethered heteroatomic picolyl-based substrate $picSPh(Me_3)$. The dioxygen reactivity of this compound was investigated and compared with that of **10**−**12**. The iron−sulfur distances in these compounds reflect the steric bulk on the Ar substituents on the picSAr ligands. Compounds containing the asymmetric carboxylate ligand are considerably less sterically hindered than those having the $\{Fe_2(O_2CAr^{Tol})_4\}$ core. Analysis of the oxidation products revealed that the yield of sulfoxide formed is controlled by the proximity of the sulfur atom to the diiron center. Although intramolecular oxidation of thioethers occurred even when the iron−sulfur distance was >4 Å, no oxidation was observed for the reaction of **6** or $[Fe_2(\mu\text{-}O_2Cbiph)_4(1\text{-}MeIm)_2]$ with external thioether substrates under the same experimental conditions.

Acknowledgment. This work was supported by Grant GM032134 from the National Institute of General Medical Sciences. E.R. is the recipient of a Schrödinger fellowship (J2485-B10) from the Austrian Science Foundation. We thank Ms. Simone Friedle for assistance in acquiring the Mössbauer spectra.

Supporting Information Available: Crystallographic refinement details, crystallographic tables (Tables S1−S3), ORTEP diagrams with atom-numbering schemes (Figures S1−S12), and X-ray crystallographic files in CIF format for complexes **2**, **3** and **5**−**14**. This material is available free of charge via the Internet at http://pubs.acs.org.

IC7014176